atmosphere

MDPI

Article

Deriving Tropical Cyclone-Associated Flood Hazard Information Using Clustered GPM-IMERG Rainfall Signatures: Case Study in Dominica

Catherine Nabukulu [1,*], Victor G. Jetten [1], Janneke Ettema [1], Bastian van den Bout [1] and Reindert J. Haarsma [2]

[1] Faculty of Geo-Information Science and Earth Observation (ITC), University of Twente, P.O. Box 217, 7500 AE Enschede, The Netherlands; v.g.jetten@utwente.nl (V.G.J.); j.ettema@utwente.nl (J.E.); b.vandenbout@utwente.nl (B.v.d.B.)

[2] Royal Netherlands Meteorological Institute (KNMI), P.O. Box 201, 3730 AE De Bilt, The Netherlands; rein.haarsma@knmi.nl

* Correspondence: c.nabukulu@utwente.nl

Abstract: Various stakeholders seek effective methods to communicate the potential impacts of tropical cyclone (TC) rainfall and subsequent flood hazards. While current methods, such as Intensity–Duration–Frequency curves, offer insights, they do not fully capture TC rainfall complexity and variability. This research introduces an innovative workflow utilizing GPM-IMERG satellite precipitation estimates to cluster TC rainfall spatial–temporal patterns, thereby illustrating their potential for flood hazard assessment by simulating associated flood responses. The methodology is tested using rainfall time series from a single TC as it traversed a 500 km diameter buffer zone around Dominica. Spatial partitional clustering with K-means identified the spatial clusters of rainfall time series with similar temporal patterns. The optimal value of $K = 4$ was most suitable for grouping the rainfall time series of the tested TC. Representative precipitation signals (RPSs) from the quantile analysis generalized the cluster temporal patterns. RPSs served as the rainfall input for the openLISEM, an event-based hydrological model simulating related flood characteristics. The tested TC exhibited three spatially distinct levels of rainfall magnitude, i.e., extreme, intermediate, and least intense, each resulting in different flood responses. Therefore, TC rainfall varies in space and time, affecting local flood hazards; flood assessments should incorporate variability to improve response and recovery.

Keywords: tropical cyclone rainfall; time series clustering; flood hazard assessment; satellite precipitation estimates; small island states

Citation: Nabukulu, C.; Jetten, V.G.; Ettema, J.; van den Bout, B.; Haarsma, R.J. Deriving Tropical Cyclone-Associated Flood Hazard Information Using Clustered GPM-IMERG Rainfall Signatures: Case Study in Dominica. *Atmosphere* **2024**, *15*, 1042. https://doi.org/10.3390/atmos15091042

Academic Editors: Qiang Dai, Shaonan Zhu and Zuntao Fu

Received: 19 July 2024
Revised: 16 August 2024
Accepted: 21 August 2024
Published: 29 August 2024

1. Introduction

Natural disasters in the Caribbean region, particularly adversities caused by tropical cyclones (TC), date back many years. The global record of natural disasters places 15 Caribbean islands in the top 25 countries most vulnerable to tropical cyclone disasters [1]. The damage costs of these small island states may be minimal on a global scale; however, citizens are often highly afflicted because the losses suffered by some of these countries exceed their economies [2,3]. Recent occurrences of TCs during the annual North Atlantic hurricane season, which includes the Caribbean region, provide increasing evidence of varied TC rainfall activity within individual storms and between storms [4–6]. This variability makes TCs capable of causing complex patterns of heavy rainfall, such that inland/riverine and flash floods are experienced at different levels of severity on the islands. In addition, the TC rainfall structure is inherently non-homogenous, characterized by a cloud system comprising rainfall bands spiralling outward from the TC centre [7] and is highly influenced by the TC's environment [8,9]. Therefore, improving long-term disaster preparedness and response strategies to account for the spatial–temporal variability of TC rainfall is essential for mitigating potential impacts.

Currently, flood hazard analysis does not take TC rainfall variability into account. The basis for disaster risk reduction (DRR) relies on estimating hazard intensities with chosen return periods. A return period analysis gives the annual exceedance probability of a hazard with a given magnitude/intensity [10]. In flooding, hazard intensity is commonly expressed as the maximum flood height in the affected area [11]. Various DRR approaches, such as engineering solutions for disaster mitigation, insurance payout, and spatial planning, all utilize simulated hazard intensities based on return periods. On the Caribbean islands, all floods are flash floods from relatively small rivers; these rivers are not gauged, and it is common to directly use the rainfall probability [12]. In the case of the Caribbean, most islands have a few stations with long records of daily data, often at locations such as airports or botanical gardens [13,14]. Apart from the scarcity of stations that may not represent the spatial variability of rainfall correctly, uncertainties in gauge measurements are attributed to the large wind speeds in tropical cyclones [15].

However, flood models need higher temporal resolutions (hourly or less than 24 h totals) to simulate all hydrological processes correctly. Thus, a statistical analysis of event shapes is necessary to create the so-called "design rainfall events" to accommodate this requirement. Several methods exist [16–18], varying from a statistical analysis of individual rainfall events of a given magnitude leading to a rainfall event that has the shape of a probability density function. Another example is an approximation, where using Intensity–Duration–Frequency (IDF) curves is followed by a method such as the Alternating Block Method (ABM) [19]. An IDF curve gives the probability of intensities for various return periods; the ABM rearranges these intensities over the period required (such as 24 h) in a slightly skewed shape, with the highest intensity in the center and the lower intensities arranged before and after.

Lumbroso et al. [20] managed to create IDF curves for some Caribbean islands for return periods of up to 1 in 50 years. However, they reported challenges related to the data quality due to incomplete and short records, and they had to combine records of various islands to generate IDF curves. While design storms provide a known probability for total rainfall depth, they often differ significantly in the temporal variation of intensities from the dynamic nature and real-world structure of TC rainfall events. Such symmetric single-peaked curves resulting from ABM may produce different flood dynamics that deviate from the realities observed during a tropical cyclone. TC rainfall exhibits concentrated heavy rain near the TC center while also spreading over large spatial extents due to outer rainbands, often without one clear peak, and is highly dynamic in space and time as the TC system translates rapidly [9,21]. An alternative source of rainfall data that is also used in early warning for tropical cyclones in the Caribbean is satellite-derived rainfall. For instance, the Global Precipitation Misson–Integrated Multi-satellitE Retrievals (GPM IMERG) offers data going back to 2000, with 30 min temporal resolution and 0.1-degree spatial resolution [22]. The ground-based rainfall derived from the radar satellite signal has its own uncertainties [23], but it still captures the spatial variability inside the precipitation system, including a tropical cyclone.

This research aims to make a first step for an alternative approach to creating design events by analyzing the spatial–temporal patterns of a TC and obtaining a reproducible method to derive statistically defined rainfall event shapes. Including the spatial–temporal variability of rainfall patterns will hopefully lead to a more effective flood hazard assessment methodology, essential for disaster preparedness and mitigation. This boils down to three questions: (1) Can a TC be characterized with one design rainfall event as is currently assumed? (2) Does a TC-derived design event (or events) resemble the commonly used design events (using IDF curves) and the rain station-measured event? (3) What does this imply for flood hazard analysis?

The developed approach applies a time series clustering analysis to the area impacted by a TC as it passes through the region of the Lesser Antilles. This essentially involves similarity measurement and grouping using clustering algorithms, presenting an opportunity for spatial–temporal rainfall pattern recognition, which is critical for reliable flood hazard

assessment [24–26]. Subsequently, a method is presented to derive cluster-based design events. These are compared to design events derived from ABM in shape and total. This study does not address the return period and is only based on a single event as a proof of concept. The next steps will involve adapting the method to multiple TCs and linking the design rainfall events to a return period.

2. Materials and Methods

The proposed three-stage workflow analyzing TCs to derive design rainfall events is presented in Figure 1. Satellite precipitation estimates over the tropical cyclone provide rainfall time series for each pixel in the study area for the selected time window. A suitable clustering algorithm clusters the rainfall time series based on their temporal behaviour. For each output cluster, a temporal alignment and quantile analysis enable the selection of 'representative precipitation signals' (RPSs) that generalize the cluster's rainfall temporal characteristics. The RPS is then the rainfall input for a flood model to examine the TC-related flood response characteristics. If similarities in flood response are observed for the RPSs, the number of optimal clusters could be reduced in the iteration of the procedure. If significant differences exist in the quantified flood characteristics, these rainfall signals are considered the best cluster RPSs, which are named TC-associate rainfall scenarios. The corresponding flooding characteristics are labelled the TC-associate flood scenarios to be used for improved and reliable TC-related flood hazard assessment. To maintain consistency with respect to risk management, the same labelling system is used, where three categories like extreme, intermediate, and least intense correspond to high, moderate, and low levels, respectively. A detailed explanation of the procedure is in Sections 2.1–2.5.

The developed workflow is tested with Tropical Storm Erika of 2015 (from here on, TS Erika), a low-category tropical cyclone that caused torrential rainfall on Dominica when crossing through the Lesser Antilles over a period from 26th to 27th August [6]. TS Erika presents a unique case study, considering its unexpected and intense rainfall. National Hurricane Center's rainfall-related advisories focused on the Leeward Islands, the Virgin Islands, Puerto Rico, the Dominican Republic, the Turk and Caicos Islands and the Southeast Bahamas, as Dominica was not anticipated to receive such severe rainfall. The local population in Dominica prepared for standard tropical storm conditions only to be surprised in the early morning by the intense rain that caused severe flooding. The majority of TS Erika's rain fell on Dominica on the 27th, reaching accumulations ranging from 300 to 700 mm recorded on ground gauges spread through the island [4,27]. The highest rain was experienced in the southern and central parts of the island; however, areas in the northern region received relatively lower rainfall totals, as reported by [28]. The intense rainfall accumulation mostly occurred within short durations of four to nine hours, thus rapidly triggering flash floods on Dominica's steep terrain [29]. The EM-DAT database reported USD 596 million in economic losses and 30 direct deaths in Dominica due to TS Erika [30].

2.1. Data Description

Half-hourly satellite precipitation estimates from NASA's GPM-IMERG Final Run Level-3 (V06) product [22] were utilized to examine TS Erika's spatial–temporal rainfall patterns. The $0.1^\circ \times 0.1^\circ$ grid dataset is satellite–gauge calibrated and is recognized by studies, e.g., [31–33], to give a higher performance in estimating rainfall extremes than other existing satellite precipitation products. The V06 reproduces the diurnal rainfall cycle and represents mesoscale convective systems with high performance [34,35]. The dataset is now widely used to monitor and provide insight into tropical cyclone rainfall patterns throughout the TC's lifespan [36–38]. Scientists have used the GPM-IMERG V06 product to combine early precipitation measurements from TRMM (2000–2015) with the latest GPM measurements to improve and grow the length of the data record [39] needed for applications such as flood hazard assessment. TS Erika's best track information obtained from the Atlantic hurricane database (HURDRAT2) of the National Hurricane Center [40] was used to determine the time window (storm duration) to download the GPM-IMERG

V06 images capturing all rainfall information needed for the analysis. The downloaded GPM-IMERG data were considered as geo-referenced time series [41], storing the recorded history of a time-evolving value (i.e., precipitation estimates) at consistent time intervals (i.e., 30 min time steps) over known locations (i.e., regular pixel grids).

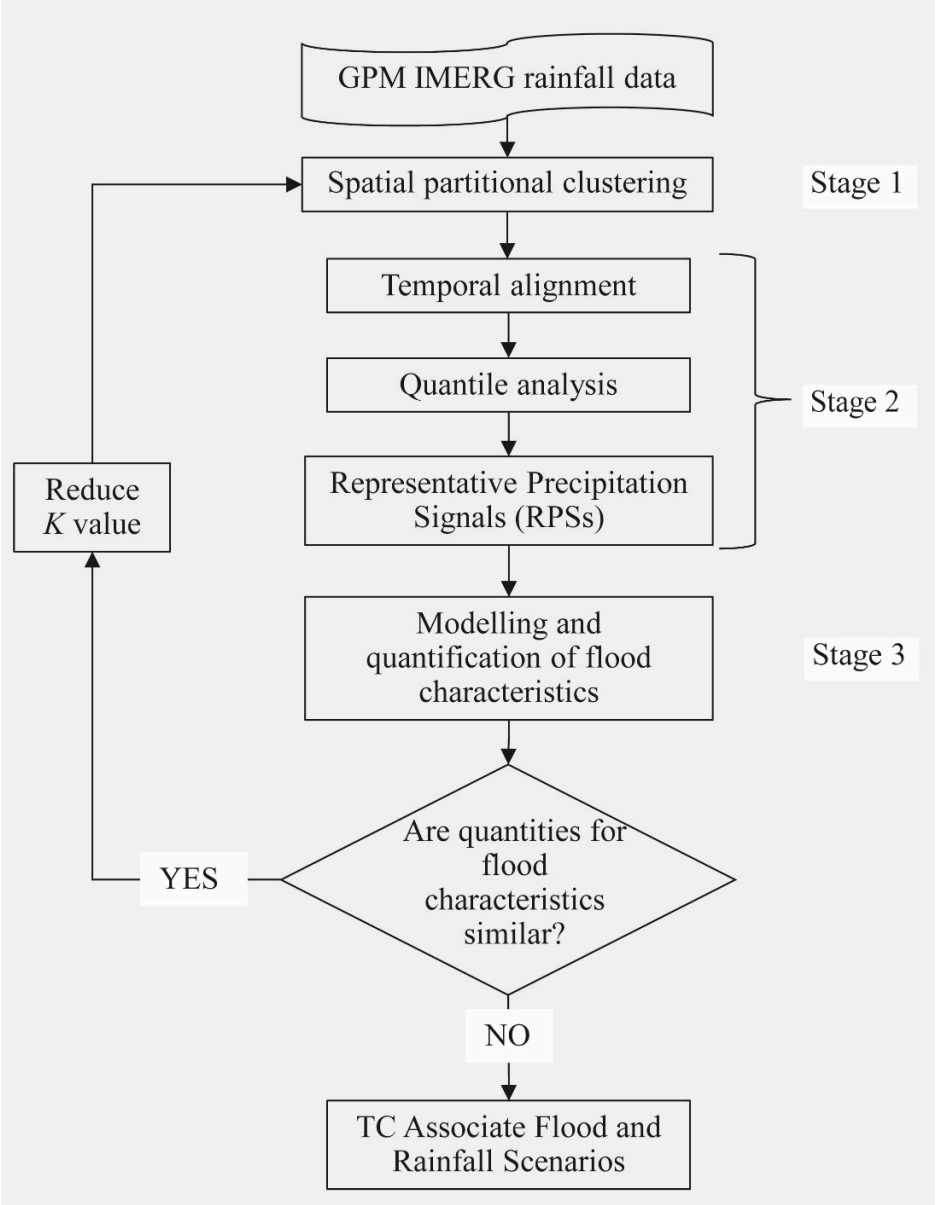

Figure 1. Flow chart for the proof of concept showing the sequence of analyses that form the developed workflow.

2.2. Spatial Partitional Clustering Using K-Means

In the first stage, the spatial partitional clustering approach explained by [42] was applied to group pixel time series into location clusters with similar rainfall temporal distributions. The K-means algorithm was used because previous research [43–45] reports the broad applicability of the algorithm for rainfall time series clustering. The optimal number of clusters (*K*) was determined using the Elbow method [46,47]. The Elbow method applies the total within-cluster sum of squares [48] as the agglomeration coefficient [49] plotted against the varying *K* values on the elbow graph. If the elbow graph is smooth and does not have a defined inflection point (elbow), the starting point of a plateau or flattening of the elbow graph indicates the distinctiveness of the output clusters [49,50]. In principle,

a good clustering should have high internal cluster compactness and external separability between the groups.

2.3. Temporal Alignment and Quantile Analysis

In the second stage, the pixel rainfall time series of the output clusters were translated into representative precipitation signals (RPSs) for input in the flood event model to predict flood response characteristics. The output clusters might be spatially distinct in the study area, introducing a challenge of varying rainfall starting periods for pixel time series in the same group since the TC was in motion, as shown in Figure 2a. To remedy the time alignment problem, the beginning of the TC's precipitation was determined by introducing a starting threshold to remove silent periods and the antecedent rain, as illustrated in Figure 2b. A given threshold value was suitable for indicating the commencement of the TC's rain if it preserved the cluster's temporal rainfall behaviour elements, i.e., the number of peaks, duration, intensity, and total volume. The less intense clusters were likely small precipitation events disparate from the tropical cyclone [51], assumed non-flood-prone and therefore excluded from further analysis. Now that the rainfall time series were at a standard onset rainfall intensity, quantile measurements of position were applied to select the representative precipitation signals, as shown in Figure 2c. As the research interest was in rainfall extremes that may trigger extreme flooding, three quantile positions, i.e., 0.5, 0.75, and 0.9, labelled $Q_{0.5}$, $Q_{0.75}$, and $Q_{0.9}$, respectively, were analyzed. The rainfall totals, intensity and duration of the quantile signals were compared to the original cluster time series to ensure that the RPSs were associated with realistic rainfall characteristics.

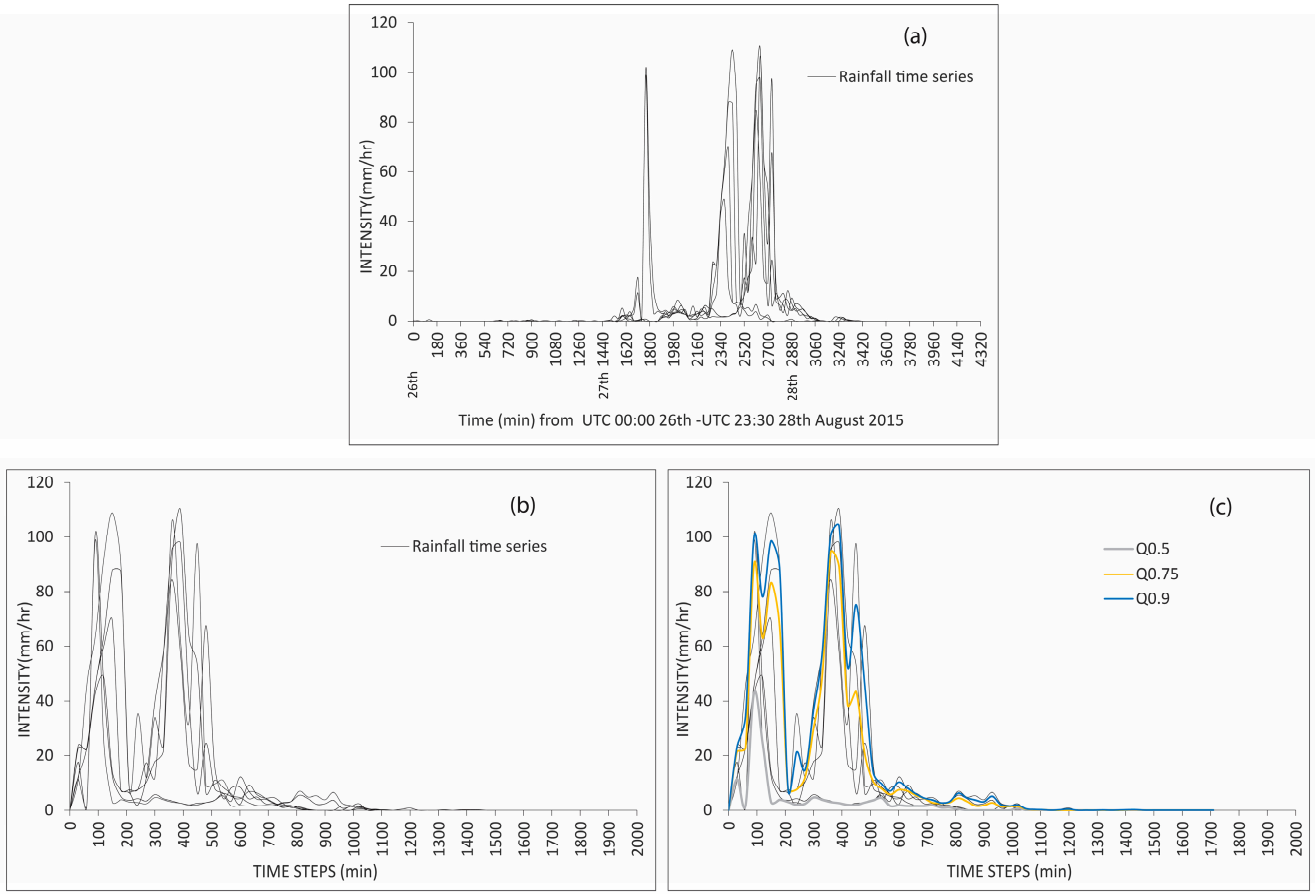

Figure 2. Illustration of the procedure for selecting cluster representative precipitation signals. (**a**) Visualization of a selection of pixel rainfall time series of a given cluster. (**b**) Rainfall series after applying a starting threshold. (**c**) Example for timestep quantile series for probabilities 0.5, 0.75, and 0.9 calculated after applying the starting threshold.

2.4. Flood Modelling

The third stage was to translate the selected cluster RPSs into flood characteristics to assess their applicability for reliable flood hazard assessment, as shown in Figure 1. The research interest was predicting the flooding, not the entire hydrological process. For each RPS, analysis was performed for flood characteristics commonly considered essential indicators for evaluating the impact of a flood hazard, i.e., flood extent, depth, volume, runoff ratio, infiltration, and duration [52]. Quantified similarities and differences in the resultant flood characteristics formed a basis for establishing the TC-associate rainfall and flood dataset. Several hydrological models have been developed, and researchers have assessed their effectiveness for flood modelling and forecasting [53–55]. This research utilized openLISEM model (www.lisemmodel.com, accessed on 31 March 2022) developed by the faculty ITC of the University of Twente (the Netherlands) to simulate the flood characteristics. OpenLISEM model is an integrated event-based hydrological model for simulating spatial–temporal processes, e.g., flooding, runoff, and sediments, on a catchment scale. The model uses representative precipitation signals (RPSs) as the rainfall input for the hydrology/flow simulation. OpenLISEM then simulates rainfall interception by vegetation and buildings and infiltration into a two-layer soil using the Green and Ampt model. Overland flow is simulated using a full Saint Venant solution for shallow floods with a finite volume semi-explicit solution [56,57]. OpenLISEM has been used successfully for flood hazard prediction in different parts of the world, for example, Uganda [58,59], Grenada [12], Dominica [60], and Spain [61], among others. The model's data requirements are described in [62] and [56]. The analysis applies model calibration parameters that have been used in existing studies over the island [63,64]. For the input database, several spatial raster data layers were assembled (20 m resolution), derived from basic maps detailed in [63], including the Digital Elevation Model (DEM), soil texture, land use/land cover, infrastructure, and rainfall.

2.5. Case Study

The testing of the newly developed workflow focused on the Commonwealth of Dominica (capital city: Roseau), an island state in the Eastern Caribbean that occupies about 750 square kilometres. Dominica is characterized by a steep and rugged landscape, with the highest peak at 1447 m in Morne Diablotins [65]. The capital Rouseau receives 2000 mm annual rainfall on average. Due to its terrain, the island experiences substantial variations in rainfall due to orographic effects [66]. Dominica is vulnerable to meteorological disasters such as torrential rainfall and powerful winds brought by tropical cyclones that form in the North Atlantic Ocean during the June to November hurricane season.

The region of interest is beyond the international boundary of Dominica, with the assumption that TC rainfall activity close to the island impacted the island's weather. The region of interest is a 500 km diameter buffer with a center on the island, as shown in Figure 3, assuming that TC rainfall activity for farther locations was likely not useful for flood hazard assessment over the island. Establishing a buffer around the island or the tropical cyclone eye is a common practice, ensuring the inclusion of the entire impact area of the TC system [67,68]. The GPM-IMERG data were downloaded for the period when the TC rainfall area was over the region of interest. The period 26 August 2015 00:00UTC to 28 August 2015 23:30UTC is the time window that captured all rainfall information required for the analysis, corresponding to the approximate time TS Erika's convective region was over the region of interest, based on the HURDAT data.

Grand Bay catchment in the south of the island of Dominica (see bottom inset, Figure 3) was selected for testing this workflow because it was severely affected by flooding due to tropical cyclone rainfall as in previous research [60,64,69]. Dominica's thin volcanic soils [70] received close to 200 mm of rainfall a fortnight before TS Erika [27]; the grounds were saturated long before TS Erika's rain, implying any additional pour likely became runoff. In this study, the initial soil moisture content was set at 85% of porosity (θi = 0.05–0.385) to allow for some infiltration. Considering Dominica's hilly terrain and the

discussion with researchers with vast experience in this study area (e.g., Victor G. Jetten), a threshold value of 0.05 m depth was set as the artificial water level to separate floods from runoff.

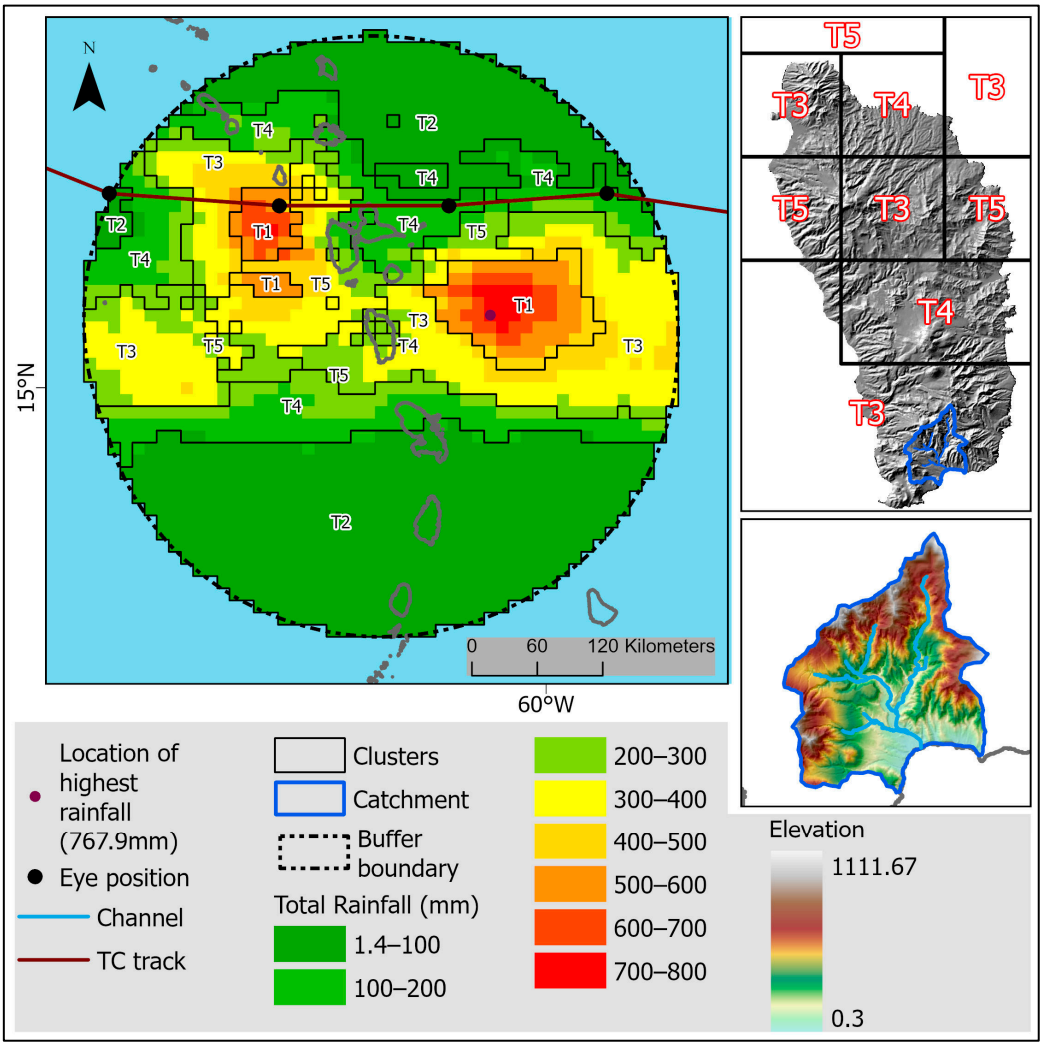

Figure 3. Map of the region of interest defined by the buffer boundary. The cumulative total rainfall for any given pixel in the study area over the selected time window is represented with a green-red colour ramp. The clusters labelled T1, T2, T3, T4, and T5 resulted from using $K = 5$ when conducting the spatial clustering analysis of the pixel rainfall time series. The bottom inset is the location of the Grand Bay catchment for which the flood modelling was performed.

3. Results

This section presents the results for the developed rainfall and flood scenarios for TS Erika based on flood modelling over Grand Bay, a small southern catchment in Dominica island state. The rainfall and flood scenarios were selected after performing two iterations of the proposed workflow in Figure 1. The labelling convention for the output clusters and their RPSs is, for instance, T1-$Q_{0.5}$ for RPS $Q_{0.5}$ of cluster T1.

The choice of the optimal value K was based on the observation of the elbow in the plot of the total within-cluster sum of squares (TWSS), a clustering goodness measure, against a range of possible K values (from 1 to 15). The output elbow graph in Figure 4 shows two sharp corners at $K = 2$ and $K = 3$, then gradually declining until $K = 5$, making it hard to pinpoint the sharp elbow. We explored clustering using $K = 2$ (too few clusters, underfitting), giving a low quality of 61.2%, while $K \geq 6$ (too many clusters, overfitting) output overlapping clusters. Thus, we selected the three values $K = 3$, 4 and 5 for an

acceptable range to evaluate clustering quality and interpretation, as shown in Figure 4. The clustering goodness measures were 83.9% for K = 5, 80.1% for K = 4, and 75.1% for K = 3.

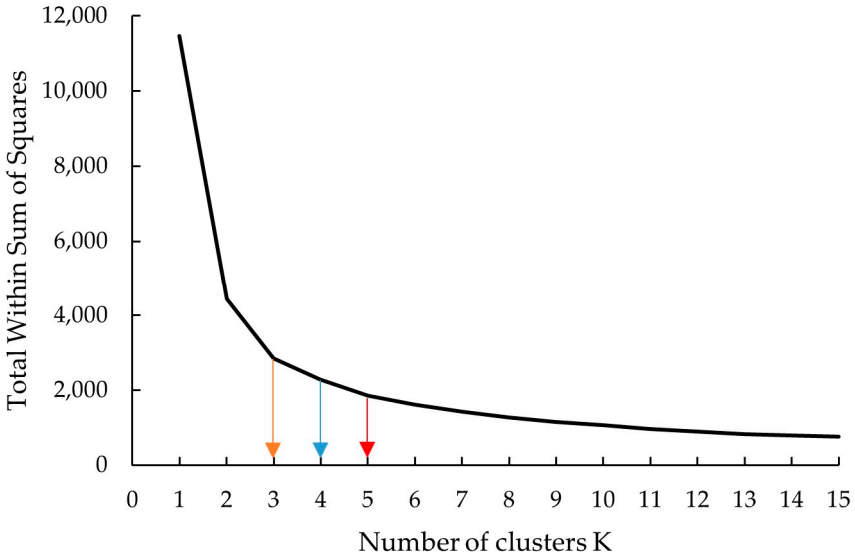

Figure 4. Elbow graph of the optimal K values used to experiment with the developed workflow. The total within-cluster sum of squares (TWSS) is the total sum of the squared distances between the data points and the centroid of their assigned clusters.

3.1. Results of the Spatial Partitional Clustering

The statistics of the spatial partitional clustering are in Table A1. With K = 5, the rainfall statistics, for instance, show that the cluster average total rainfall decreased in the order of T1, T3, T5, T4, and T2. Pixels with the highest precipitation are in two spatially distinct regions of cluster T1, mainly concentrated south of the storm track and over the ocean, as shown in Figure 3. This spatial dissimilarity was also observed in other clusters, such as T2, comprising pixels far (north and south) from TS Erika's track. At this point, pixels over Dominica are in clusters T3, T4, and T5, as shown in the top inset in Figure 3. The Grand Bay catchment is located in cluster T3. T2 was the largest cluster, including 41.8% of the rain pixels, with very low rainfall intensity and volume.

In the first iteration with optimal clusters K = 4, the pixel time series redistributed to form four spatial clusters as shown in Figure A1. The cluster extremes (in terms of the total rainfall and intensity) decreased in the order of T1, T3, T4, and T2, as shown in Table A1. T1 is the most extreme and T2 is the least intense cluster. There is a similar range for maximum rainfall intensity for clusters T1 and T2 in both cases of using K = 5 and K = 4; however, there were slight changes in total rainfall for both clusters. The pixels that comprised T5 when using K = 5 were possibly redistributed into other clusters, hence the slight changes in the cluster statistics when using the optimal value K = 4. At this point, pixels over Dominica are in clusters T3 and T4.

The second iteration of the workflow with the optimal value K = 3 outputs three spatial clusters with quantified rainfall extremes reducing in the order T1, T3, and T2, which is also presented in Table A1. Compared to using K = 5 and K = 4, pixels merged further to form the three clusters (see Figure A1), hence the larger cluster size, especially for T2 and T3. The range of the maximum rainfall intensity did not change for the most extreme cluster, T1. Compared to results from using K = 5, there were observable changes in the total rainfall associated with the output clusters. Further merging of the pixels influenced the average total rainfall of the individual clusters and the significant difference in the cluster boundaries, especially for T3.

In all three experiments, the cluster statistics for T2 showed shallow ranges of the calculated rainfall characteristics, and the cluster was at the outer edges of the area of

interest. As explained in Section 2.3, rainfall over T2 pixels was assumed not associated with TS Erika; hence, pixels of this cluster were excluded from further analysis.

3.2. Cluster Representative Precipitation Signals

After disregarding T2, the temporal alignment and quantile analysis for the remaining clusters derived representative precipitation signals (RPSs) for running openLISEM flood model over the Grand Bay catchment. When the beginning of the storm's precipitation was varied for four intensity values, i.e., 2, 5, 10, and 20 mm/h, the intensity of 10 mm/h was the most appropriate to align the time series for the onset of TS Erika's rainfall. For the first experiment applying $K = 5$, derived RPSs for clusters T1, T3, T4, and T5 at quantile positions, i.e., $Q_{0.5}$, $Q_{0.75}$, and $Q_{0.9}$ are plotted in Figure 5. The corresponding rainfall characteristics are in Table 1. The signals derived at $Q_{0.9}$ were unrealistic; their quantified total rainfall was way higher than the totals for the original time series. Therefore, only $Q_{0.5}$ and $Q_{0.75}$ were the selected RPSs for the individual clusters resulting from $K = 5$.

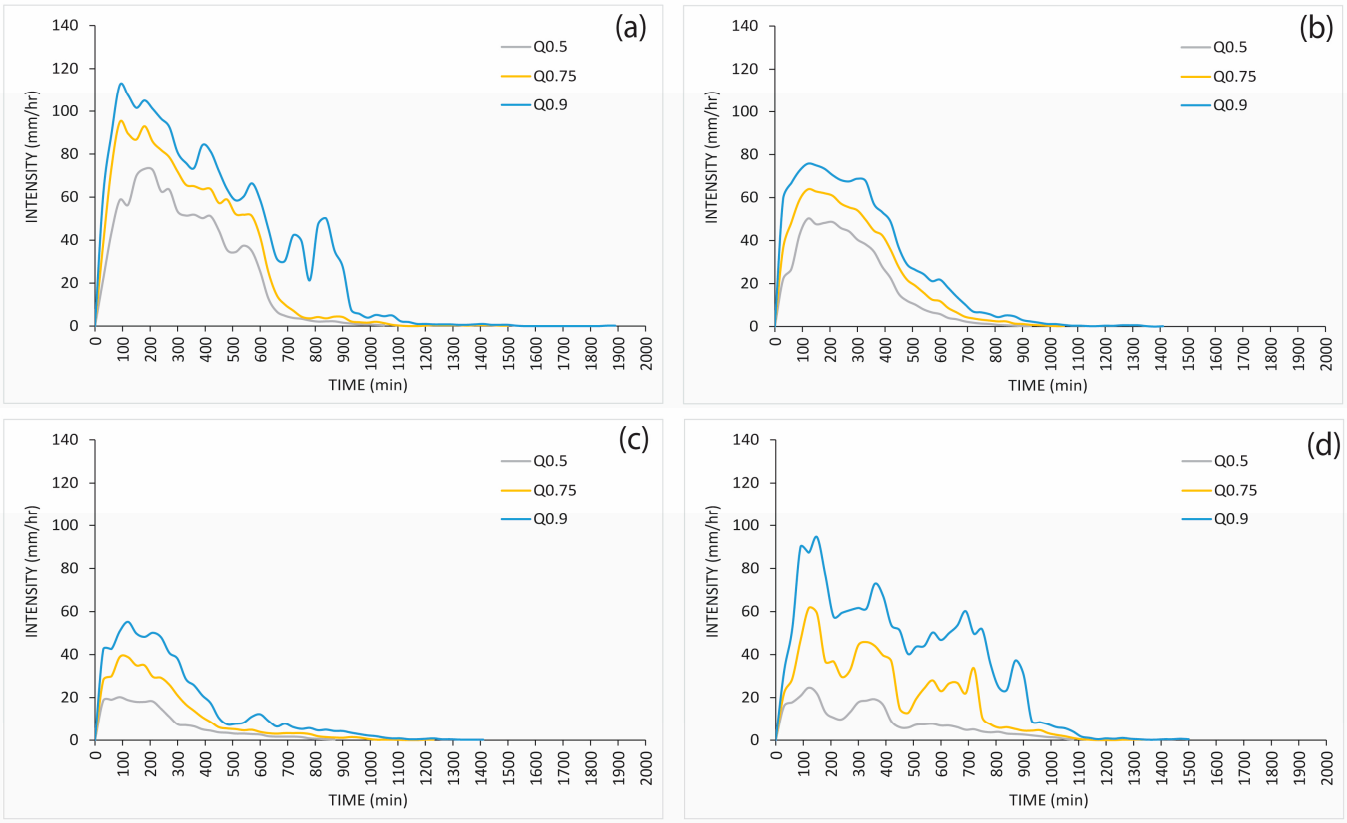

Figure 5. The outcome of the time alignment and quantile analysis when applying $K = 5$. Only $Q_{0.5}$ and $Q_{0.75}$ were selected for each cluster as the representative precipitation signals (RPSs). Clusters T1, T3, T4, and T5 are in graphs (**a**), (**b**), (**c**), and (**d**), respectively.

In Figure 5, RPSs for clusters T1, T3, and T4 had similar shapes; however, the signals differed significantly in duration, cumulative rainfall, and maximum intensity, as shown in Table 1. The T5 RPSs comprised multiple peaks with relatively low rainfall intensity. Notably, the flood response showed a higher result for $Q_{0.75}$, as detailed in Section 3.3. Consequently, for the $K = 4$ and $K = 3$ clusters, the analysis exclusively derived RPSs at $Q_{0.75}$ for subsequent flood model simulations. When using $K = 5$, eight RPSs are applied to run the flood model. By applying only $Q_{0.75}$, the analysis yields three RPSs for $K = 4$ and two RPSs for $K = 3$. The derived RPSs for clusters resulting from the second iteration applying $K = 3$ were associated with lower values for the rainfall characteristics than when using $K = 5$ and $K = 4$.

Table 1. Rainfall statistics for RPSs $Q_{0.5}$, $Q_{0.75}$, and $Q_{0.9}$ for the spatial clusters. Only $Q_{0.5}$ and $Q_{0.75}$ were used to run the flood model in the first experiment, applying $K = 5$. For iterations applying $K = 4$ and $K = 3$, only RPS $Q_{0.75}$ is derived to run the flood model. T_r is total rainfall, I_{max} is maximum intensity, and D_r is duration.

***K* = 5**												
	T1			**T3**			**T4**			**T5**		
RPS	T_r (mm)	I_{max} (mm/h)	D_r (h)	T_r (mm)	I_{max} (mm/h)	D_r (h)	T_r (mm)	I_{max} (mm/h)	D_r (h)	T_r (mm)	I_{max} (mm/h)	D_r (h)
$Q_{0.5}$	518.9	73.1	17.5	307.1	50.2	15.5	107.6	20.2	14.5	159.7	24.6	18.0
$Q_{0.75}$	729.9	94.9	25.0	440.0	63.8	17.5	209.9	38.9	20.5	427.3	61.6	22.5
$Q_{0.9}$	1029.1	112.4	31.5	587.0	75.8	23.5	345.3	55.2	23.5	834.9	94.5	25.0
***K* = 4**												
	T1			**T3**			**T4**					
	T_r (mm)	I_{max} (mm/h)	D_r (h)	T_r (mm)	I_{max} (mm/h)	D_r (h)	T_r (mm)	I_{max} (mm/h)	D_r (h)			
$Q_{0.75}$	727.3	91.4	25.0	446.2	65.0	18.0	230.4	42.2	18.0			
***K* = 3**												
	T1			**T3**								
	T_r (mm)	I_{max} (mm/h)	D_r (h)	T_r (mm)	I_{max} (mm/h)	D_r (h)						
$Q_{0.75}$	676.6	84.9	24.5	381.3	59.0	17.5						

3.3. Results for the Flooding Simulations

3.3.1. RPSs from K = 5

For the RPSs resulting from the first experiment when applying $K = 5$, the quantities of the flood simulations for eight separate runs of the openLISEM model are given in Table A2 for the clusters T1, T3, T4, and T5. Eight quantities (two for each cluster) are recorded for each flood characteristic, e.g., the flood extents due to RPSs T1-$Q_{0.5}$ and T1-$Q_{0.75}$ are 3.98 km^2 and 4.84 km^2, respectively. The eight RPSs caused flood extents ranging from 1.02 to 4.84 km^2. On average, T1 and T3 signals caused larger flooded extents with water at greater depths ranging from 2.79 to 4.21 m (see Table A1), which is attributed to the high rainfall intensity of these RPSs. RPSs that caused large flood volumes (i.e., in the range of 1.10 to 2.28 million m^3) consequently generated a high runoff ratio (above 0.7). Infiltration was generally low for all RPSs, resulting in long flood durations ranging from 15.71 to 27.24 h.

The quantified flood characteristics of the individual RPSs were further examined for differences and similarities. There were across-cluster similarities; for instance, T3-$Q_{0.5}$ and T5-$Q_{0.75}$ caused the same flood extent. Also, the flood depth and volume of these RPSs could be regarded as similar responses, considering the minor differences in the quantities. RPSs T1-$Q_{0.5}$ and T3-$Q_{0.75}$ also exhibited similarities in their flood quantities; for example, the flood depth only differed by 0.18 m, which could be considered minimal in flood hazard assessment. Only infiltration and flood duration showed significant differences across all RPSs and clusters. $Q_{0.75}$ generated the highest quantities of the calculated flood characteristics for all clusters compared to $Q_{0.5}$. There was a strong linear correlation between the flood (extent, duration, volume, runoff ratio, and infiltration) and rainfall (cumulative total and maximum intensity) characteristics with correlation coefficients in the range of $0.85 < r < 0.98$. However, the maximum rainfall intensity was a dominant driver of the flood responses, considering that precipitation curves for clusters T1 had the highest rainfall intensity and flood characteristics. In contrast, the lowest rainfall intensity and flood quantities were associated with T4.

The observed similarities in the quantified flood characteristics for the RPSs belonging to supposedly different clusters signified the likelihood of redundancy during the clustering

phase of the rainfall time series. The value $K = 5$ was an arbitrary choice since the elbow graph did not give a defined inflection point, as shown in Figure 4. However, choosing $K = 5$ helped define a starting K value for the first experiment. To examine the effect of this choice, two iterations of the procedure in Figure 1 were performed by reducing the optimal clusters to $K = 4$ and $K = 3$ before conducting the spatial partitional clustering again. Only the $Q_{0.75}$ was derived for both iterations, considering the RPS had enormous quantities for the investigated flood characteristics across all the clusters when using $K = 5$.

3.3.2. RPSs from K = 4 and K = 3

The simulated flood responses for RPSs resulting from applying $K = 4$ and $K = 3$ are presented in Table 2. With $K = 4$, quantified differences in flood characteristics of the three $Q_{0.75}$ RPSs show that T1caused more 1.09 km^2 of the flooded extent than T3. Also, the flood duration for T3 was shorter than that for T4 by 10.17 h. When compared to results from using $K = 5$, there were substantial differences in the flood characteristics of the RPSs for clusters from $K = 4$. Three levels of variation in the order T1, T3, and T4 for both the rainfall and flood characteristics were observed. For example, the maximum rainfall intensity (mm/h) is 91.4, 65, and 42.2 for T1, T3, and T4, respectively. The three RPSs are also associated with flood depths with significant differences in Figure 6. For the two RPSs using $K = 3$, the simulated flood response output quantities are slightly lower than those for RPSs using $K = 4$ (see Table 2). For instance, the flood extent of the most extreme cluster T1 when using $K = 4$ is 4.80 km^{2,} and when using $K = 3$, the flood extent is 4.62 km^2.

Table 2. Calculated flood characteristics for RPSs Q0.75 resulting from using $K = 4$ and $K = 3$.

***K* = 4**						
	Flood extent (km^2)	Flood depth (m)	Flood volume (million m^3)	Runoff ratio	Infiltration (mm)	Flood duration (h)
T1	4.80	4.22	2.22	0.85	98.13	23.73
T3	3.70	3.65	1.42	0.77	88.95	19.16
Diff	1.09	0.57	0.79	0.08	9.18	4.57
T1	4.80	4.22	2.22	0.85	98.13	23.73
T4	2.47	1.84	0.84	0.62	74.08	29.33
Diff	2.32	2.39	1.38	0.23	24.06	−5.61
T3	3.70	3.65	1.42	0.77	88.95	19.16
T4	2.47	1.84	0.84	0.62	74.08	29.33
Diff	1.23	1.82	0.59	0.15	14.87	−10.17
***K* = 3**						
	Flood extent (km^2)	Flood depth (m)	Flood volume (million m^3)	Runoff ratio	Infiltration (mm)	Flood duration (h)
T1	4.62	4.18	2.05	0.84	97.69	22.76
T3	3.48	3.35	1.28	0.74	84.40	20.83
Diff	1.14	0.83	0.77	0.10	13.29	1.93

3.4. Selection of Final Rainfall Scenarios for TS Erika

The decision on final rainfall and flood scenarios for TS Erika was based on the detailed examination of the outputs from the iteration of the workflow in Sections 3.1–3.3. After further reducing the optimal clusters, the two RPSs from $K = 3$ resulted in an overgeneralization of the rainfall statistics. For instance, the cluster size of the most intense cluster (T1) became larger than that for $K = 4$, as shown in Table A1. The effect of the generalization is also depicted in the lower rainfall intensity and totals associated with RPSs from $K = 3$ in Table 1. The RPSs from $K = 4$ reveal three existing levels of rainfall variation that were otherwise merged and oversimplified by $K = 3$. The value $K = 4$ gave a more realistic partition of the pixel rainfall time series since it dissolved the redundant cluster T5, as

shown in Section 3.1 and Figure A1, without significantly altering the rainfall statistics and boundaries of the clusters.

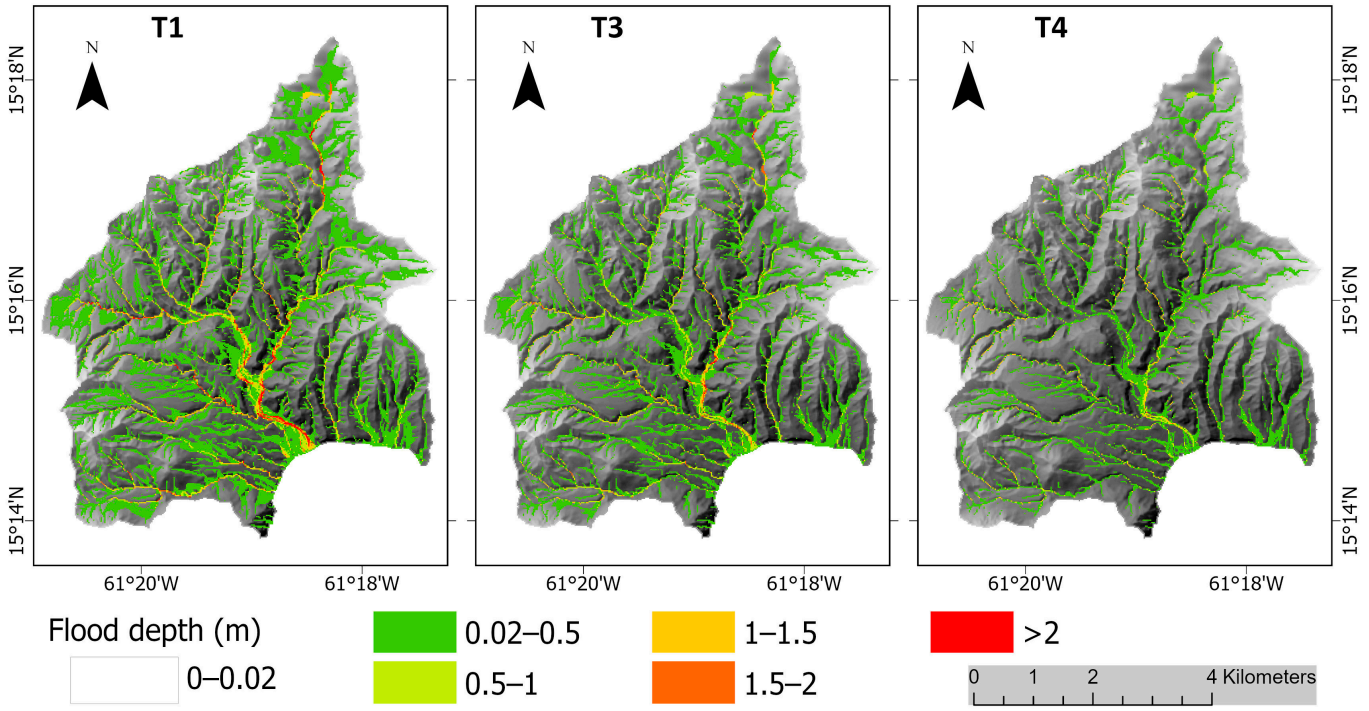

Figure 6. Flood depth maps for Grand Bay catchment on Dominica as simulated using the $Q_{0.75}$ RPSs for clusters T1, T3, and T4 resulting from applying $K = 4$.

The RPSs for both iterations $K = 4$ and $K = 3$ resulted in significantly different quantified flood characteristics, unlike the $K = 5$ signals, which gave a redundancy. However, the RPSs for $K = 4$ had a higher flood impact than $K = 3$; therefore, the $Q_{0.75}$ signals from $K = 4$ were a reliable representation of TS Erika's rainfall scenarios. The three levels of variation were labelled as extreme (T1), intermediate (T3), and least intense (T4), as shown in Figure 7. The associated flooding characteristics in Table 2 were TS Erika's flood scenarios.

3.5. Comparison

For comparison, the analysis used the average hourly rainfall in Dominica due to TS Erika from Table 1 of the report by [28] and IDF curves generated by [20].

The analysis uses the average because every station provides a different measurement depending on its location on the island and which part of the cyclone passed over the station. Also, the average is usually the best available measurement applied in hazard analysis. For instance, Ogden [27] utilized island-wide radar-based average rainfall to run the GSSHA model on 16 watersheds in Dominica to simulate peak discharges during TS Erika. However, these averages do not capture the natural variability of the TC rainfall. In the case of TS Erika, the measured average rainfall in Figure 8a was similar (in rainfall totals) to the intermediate rainfall scenario Figure 7b from the clustering analysis. However, TS Erika showed three distinct rainfall scenarios, each potentially resulting into different flood responses upon reaching the island.

The IDF curves generated by [20] were used to create a design storm by applying the Alternating Block Method [19] based on 30 min time steps like the GPM-IMERG. In Figure 8b,c, the IDF-based design events have much lower rainfall totals, quite different from the cluster-based design events. Also, the rainfall intensity, duration, and shape of the IDF-based design events are very different from those of station-based and cluster-based storms. These differences influence the modelled flooding processes.

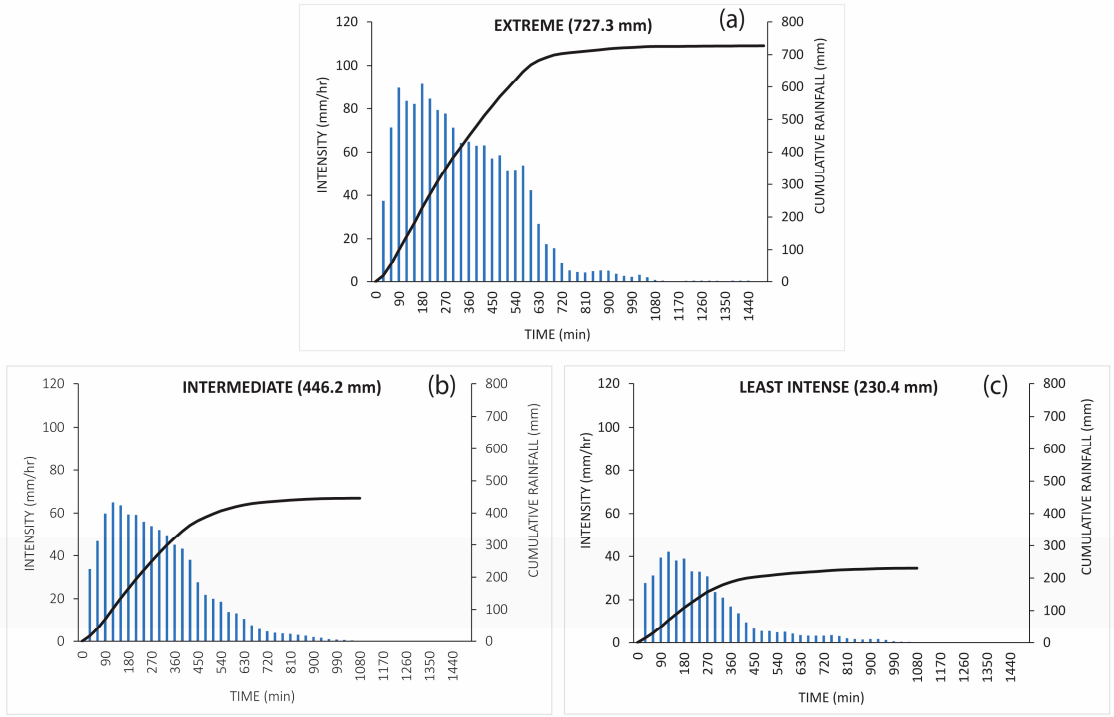

Figure 7. Precipitation time series (intensity/duration) and cumulative plots of the TC-associated rainfall scenarios for TS Erika resulting from $K = 4$. The blue bar graphs represent the half-hourly rainfall intensities, and the black line is for the cumulative precipitation. (**a**) Extreme, (**b**) intermediate, and (**c**) least intense.

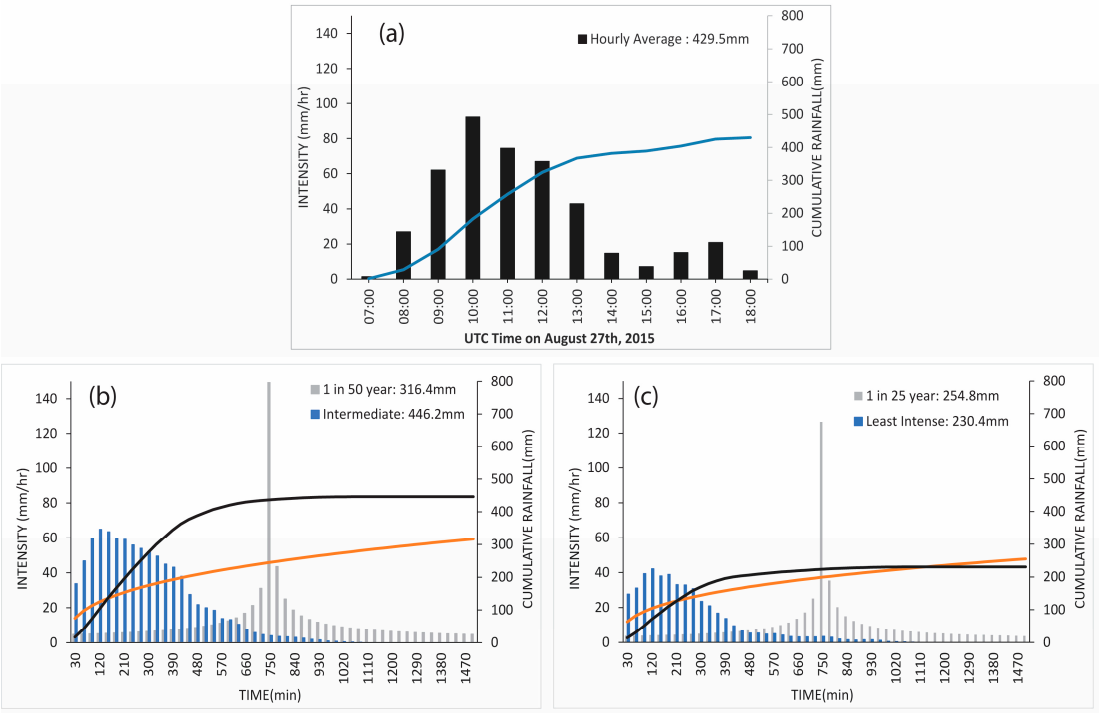

Figure 8. Plots of (**a**) the average hourly rainfall on Dominica due to TS Erika and the line plot of the cumulative rain from Table 1 of the report by [28]. Plots (**b**,**c**) compare the output cluster-based design events with the design storms derived from IDF curves available for the region in Figure 3 from [20] by applying the ABM. The line plots (**b**,**c**) are the corresponding cumulative rainfall, black for the output cluster-based design events and orange for the design storms.

4. Discussion: Final Rainfall Scenarios for TS Erika

The current study establishes a three-stage approach that uniquely combines three methods, spatial partitional clustering, quantile analysis, and flood modelling, to generalize the rainfall (sourced from satellite imagery) of a tropical cyclone toward improved flood hazard assessment.

The variables applied in stage 1 of the workflow, as shown in Figure 1, to run the clustering algorithm, such as quartiles (e.g., $Q_{0.5}$, $Q_{0.75}$, $Q_{0.9}$), total rainfall, and mean and standard deviation of rainfall rate, are recognized in the literature [71,72] among the features used for rainfall event characterization. K-means gave a high performance for the rainfall time series clustering with a high partitioning quality detecting the different rainfall spatial–temporal patterns within the tropical cyclone. The K-means already produced a good clustering when delineating spatial regions for seasonal precipitation [73]. Another study [74] reports the clustering quality of K-means when applied to detect the presence of cumulative rainfall spatial patterns in the rainfall of typhoons that impacted a catchment on a tropical island.

The choice of the optimal number of clusters was essential to the research because the rainfall characteristics were classified based on the K value. Using a too-high value enhances redundancy in flood scenarios, and a very low K value might overmerge and generalize the data. For instance, there was redundancy when using $K = 5$ and excessive data merging when using $K = 3$. The reduction in the K value shows that the spatial–temporal distribution of TC rainfall characteristics does not have definite cluster boundaries, as some pixels moved from one cluster to another. The absence of stable cluster boundaries of the rainfall characteristics is attributed to the change in the environment that the storm encountered while in motion, influencing how rainfall was distributed around the eye from time to time.

The storm was in motion, and some regions experienced comparable rainfall magnitudes even when these places were far from each other, as revealed by the spatial partitional clustering. Setting a threshold to separate TC and non-TC components proved important for the quantile analysis (in stage 2) as the rainfall time series would be aligned based on the moment when the TC-associate rainfall began. Previous research [75–77] suggests a 5 mm/h threshold to delineate regions of TC-associated rainfall for areas such as the Eastern United States, the Western Gulf of Mexico, and the Caribbean Sea. However, Dominica generally experiences much more rainfall than these regions, even outside the hurricane season.

In Dominica, rain rates of $\leq$5 mm/h could potentially be associated with other weather events, not TCs. The study applied a 10 mm/h threshold, which was realistic for defining the start of TS Erika's rainfall for all three experiments. This threshold brought back TS Erika's rainfall temporal behaviours, i.e., a steep increase, then the rain dying down after a period of heavy pour [4,28]. The threshold was essential to remove the antecedent rain, unrelated to the tropical cyclone, and to give insight into initializing the flood model (in stage 3), especially the initial soil moisture content. The antecedent rainfall (whether TC-related or not) makes the catchment wetter and decreases the storage capacity, eventually inducing runoff water.

The selection of the cluster RPSs was based on aggregated statistics computed across all the time series at each timestep rather than individual pixel rainfall realizations. This approach aimed to identify an acceptable range of time series that best represented the collective temporal patterns of the entire cluster. As recommended by [72], the analysis applied the quartile positions at $Q_{0.5}$, $Q_{0.75}$, and $Q_{0.9}$ in the first experiment when using $K = 5$. Analysis of the aggregated rainfall statistics showed unrealistic quantities at $Q_{0.9}$ that were not comparable with the original rainfall time series statistics, and thus, only $Q_{0.5}$ and $Q_{0.75}$ best represented the cluster temporal patterns.

In stage 3, the simulated flood characteristics for the selected $Q_{0.5}$ and $Q_{0.75}$ RPSs when using $K = 5$ revealed two key observations: (1) intra-cluster similarities in the quantified flood characteristics for the RPSs and (2) $Q_{0.75}$ causing larger quantities of the flood charac-

teristics than $Q_{0.5}$. These observations motivated the decision to introduce an iteration of the workflow for a reduced value of *K*. The research interest was in TC extreme rainfall and flood characteristics towards a flood hazard assessment; hence, only the RPS $Q_{0.75}$ was derived and applied to run the flood model, which is in line with a study by [25] also suggesting that a threshold at the upper quantile (75%) was more representative of cluster flood-generating precipitation. Two iterations of the procedure provided more outputs and options as a basis for a logical decision of the final rainfall scenarios and the associated flood characteristics.

We realize that the third step of the method, flood modelling, depends on the local circumstances of an island and the flood model used. This could be seen as an advantage: the design events selected are closely related to the hazard and its location. However, it may also be a disadvantage as the capacity for flood modelling must be present, and the results may depend on the catchment modelled and highly local circumstances. Moreover, there are other hydrological hazards, such as landslides and debris flows, that have different and more complex models. The step is presented as a possibility; further research can show if this is a necessary step.

An advantage of this method is that it follows the TC as it passes in the region and is not tied to a gauge location. One could argue that this better characterizes the TC. However, the T1 cluster total rainfall is very high. For this particular storm, the extreme rainfall of cluster T1 relates to the hotspots over the ocean, none of which reaches Dominica. Both T1 hotspots were south of the TC track, and reports [4,28] also show that TS Erika's heavy rain was located south of the storm. Future investigations should explore whether such extremes are consistently directed towards the ocean and if the islands regularly encounter rainfall of similar magnitude. The intermediate (T3) and least intense (T4) are within the ranges of the cumulative totals observed in Dominica. For instance, data by [28] recorded 24 h rainfall totals for nine ground stations ranging from 217.9 mm to 493.6 mm across the island. The maximum rainfall rate of 122.6 mm/h was observed at Grand Fond. The station at Grand Bay recorded 481 mm of cumulative rain with a maximum intensity of 94.6 mm/h. Before TS Erika, the station at Melville Airport reports Tropical Cyclone Ivan in 2004 as the highest on the island, with 422 mm in 24 h, between 1976 and 2013 (unpublished data). The selected final RPSs summarize the cluster temporal patterns, but there can be variations within the clusters (see Table A1).

This research does not invalidate gauge-based IDF curves if there are location-specific curves present. However, in Figure 7, the study highlights that in the flood hazard assessment of tropical cyclones, there is an inherent spatial–temporal variability in rainfall that IDF curves may not fully represent. Only when there are sufficiently detailed rainfall measurements in an area, such as a series of tipping bucket stations, could spatial variability be captured. Additionally, the current analysis does not address return periods nor remodel the flood impact in Dominica during TS Erika. Instead, we use TS Erika as an example to develop a more holistic approach to characterize TC rainfall spatial–temporal patterns and improve flood hazard assessments.

The duration, shape, and intensity of the final RPSs differ from the representations given by the design storms from existing IDF curves, as shown in Figure 8. Design storm curves are associated with a single peak and a duration that is adapted to reach a total storm depth based on a given return period. From Figure 8, it is clear that the shape, peak intensity, timing of the peak, and duration are very different from the real rainfall and from the cluster-derived events. We did not simulate the flood for the IDF-based design storm because of the difference in magnitude from the cluster-based events. The IDF-based storm is related to a given recurrence interval with related magnitudes. If we succeed in evolving our method to more tropical cyclones so that we can assign a return period, a better comparison may be possible.

A return period analysis is normally related to one location, giving a magnitude and its exceedance probability for that location. A different station on the island would have a different frequency magnitude analysis. The highest values, however, could be part of

the same TC with the same probability of rainfall as the same system. It would be better to know the return period of a given TC and accept that there is a range of rainfall magnitudes within it, with different events that characterize it.

The strength of the developed method is that it only focuses on tropical cyclone rainfall, so a given location can prepare for a TC, for instance, when IDF curves are not available. However, there are issues to solve. We recognize fully that satellite data (the GPM-IMERG) is not ground truth. We are aware that the GPM-IMERG half-hourly may not be the best product; the data description highlights problems with the quality of the 30 min intensities [39]. The dataset is calibrated based on monthly gauge totals; the constellation of satellites registers three hourly data and interpolates to 30 min images [22]. This leads to deviations from ground-measured rainfall. There is no ground data strong enough to calibrate the satellite data on Dominica at the moment. A significant strength of the GPM-IMERG is the significant potential to give measurement information when there are no rainfall gauges. Finally, ground stations under storm and cyclone circumstances are subjected to windspeeds of 120–240 km/h, so 'ground truth' in this context is also subjective.

5. Conclusions

This research shows an innovative three-stage methodology to improve how adequate estimates of TC-specific rainfall can be summarized and accurately fed into flood simulations. The developed method reveals that spatial variability exists for the same TC rainfall event and should be accounted for to achieve a reliable flood hazard assessment. TC rainfall is complex, so for the on-ground flood hazard, it matters which part of the cyclone passes over an area. Because rainfall patterns vary within a single TC, there is not one rainfall curve that should represent a tropical cyclone. This realization makes hazard analysis more complex as it now involves a choice in a (limited) set of curves, with the possibility to 'define a worst-case scenario' based on the highest rainfall cluster.

The shape, intensity variation, and duration of these cluster-derived events are much closer to actual rainfall than the IDF-derived events, thus providing an adequate representation of TC-associated rainfall for simulating potential hazards. The research findings highlight the importance of detailed characterization of TC rainfall; for instance, with the simulated flood maps, various hazard scenarios are created to better prepare for potential locally differing impacts from the same TC. Identifying areas with the most significant impacts from the TC rainfall ensures the fastest emergency response and helps responders determine the safest routes to reach vulnerable populations. This integration of spatial and temporal rainfall patterns into flood hazard assessments is a crucial step forward in improving the resilience of communities to TC-induced flooding.

The IDF-derived event, in this case, is based on a scarce dataset, while the satellite images simply cover the entire TC impact area. Thus, in the absence of long-term rain gauge measurements, it is shown that the developed method can be used as it exploits the potential of satellite precipitation estimates (e.g., higher temporal resolution and wide coverage) in capturing TC rainfall measurements. Unlike the IDF curves based on long-term temporal data on one location, the method developed here has the advantage that the RPSs of the analyzed TC are established based on all available satellite rainfall data in the study area during the period of the storm. Therefore, this method does not depend on short and potentially incomplete datasets from ground measurements or IDF curves that are borrowed from other regions (e.g., neighbouring islands). In an area of scarce data, our method could be a solution.

The current research represents a first attempt where we examine a single tropical cyclone. In future studies, the approach will expand to include multiple tropical cyclones and islands, although this is beyond the scope of this paper. Risk reduction requires a probability assessment of the rainfall, for which we do not have a method yet. The approach should be moved forward because it is simple, uses high-resolution satellite data and would improve risk assessment when the probability is addressed. The research methodology is not confined to Dominica; rather, the island is a proof of concept. Thus, the developed

method can be tested and applied in other tropical cyclone-prone regions in other oceanic basins, considering that TC systems all form the same way, though the designations and direction of rotation differ by geographical location.

However, the method is currently experimented on one tropical cyclone; we need to extend to more TCs to include all the different categories before it is usable. Each TC exhibits a different rainfall pattern in time and space, which can be a challenge for this approach. Linking the representative precipitation signals to flood hazard assessments may require further generalizing, such as re-clustering the rainfall scenarios across multiple TCs. To address this, we recommend involving local stakeholders in disaster risk reduction, like the Dominica Meteorological Service. Local experience can help ensure rainfall scenarios are accurately tailored to their island, leading to better decision-making, preparation, and mitigation.

Author Contributions: C.N., V.G.J. and J.E. contributed to the study's conception, design, and methodology. C.N. performed material preparation, data collection, and analysis. R.J.H. contributed to the interpretation of the rainfall data. B.v.d.B. was involved in flooding modeling and interpretation of results. C.N. wrote the first draft of the manuscript, and all authors commented on previous versions. All authors have read and agreed to the published version of the manuscript.

Funding: This research received no external funding.

Institutional Review Board Statement: Not applicable.

Informed Consent Statement: Not applicable.

Data Availability Statement: The data presented in this study are available on request from the corresponding author due to privacy.

Conflicts of Interest: The authors declare no conflicts of interest.

Appendix A

Table A1. Summary statistics for the output spatial clusters.

		***K* = 5**				
Cluster		T1	T2	T3	T4	T5
Cluster size		132	798	433	399	149
%		6.9	41.8	22.7	20.9	7.8
Maximum intensity (mm/h)	min	55	0.4	36.4	18.2	32
	max	120	50.2	120	111	120
Total rainfall (mm)	min	451.5	1.4	201.1	47.8	121
	max	767.9	112.4	571.5	275.9	603.2
	mean	583.9	29.4	344.2	167.5	331.4
		***K* = 4**				
Cluster		T1	T2	T3	T4	
Cluster size		146	818	513	434	
%		7.6	42.8	26.8	22.7	
Maximum intensity (mm/h)	min	55	0.4	42	18.8	
	max	120	50.2	120	111	
Total rainfall (mm)	min	433.7	1.4	202.2	47.8	
	max	767.9	132.1	571.5	275.9	
	mean	574.3	31.1	347.6	180.1	
		***K* = 3**				
Cluster		T1	T2	T3		
Cluster size		212	937	762		
%		11.1	49.0	39.9		
Maximum intensity (mm/h)	min	55	0.4	26		
	max	120	68.6	120		
Total rainfall (mm)	min	352.5	1.4	83.6		
	max	767.9	171.9	489.2		
	mean	530.8	42.7	279.8		

Table A2. Calculated flood characteristics for RPSs $Q_{0.5}$ and $Q_{0.75}$ resulting from using K = 5.

RPS	T1	T3	T4	T5
Flood extent (km^2)				
$Q_{0.5}$	3.98	3.12	1.02	1.40
$Q_{0.75}$	4.84	3.76	2.19	3.12
Flood depth (m)				
$Q_{0.5}$	3.88	2.79	1.26	1.32
$Q_{0.75}$	4.21	3.70	1.69	2.85
Flood volume (million m^3)				
$Q_{0.5}$	1.67	1.10	0.42	0.56
$Q_{0.75}$	2.28	1.50	0.77	1.12
Runoff ratio				
$Q_{0.5}$	0.80	0.71	0.33	0.43
$Q_{0.75}$	0.85	0.77	0.59	0.74
Infiltration (mm)				
$Q_{0.5}$	92.14	75.31	60.83	77.82
$Q_{0.75}$	97.42	86.61	73.03	98.50
Flood duration (h)				
$Q_{0.5}$	18.43	15.71	16.68	23.64
$Q_{0.75}$	27.24	18.85	22.25	18.60

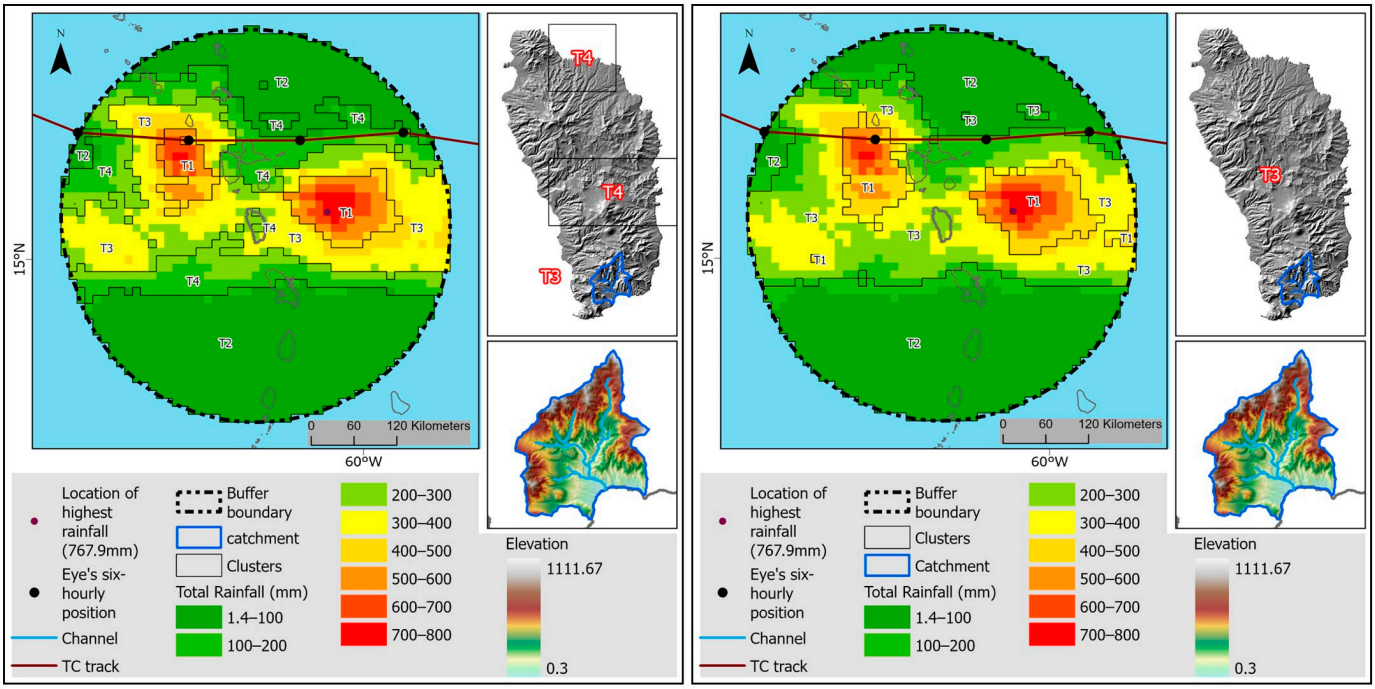

Figure A1. The maps below represent the cluster boundaries resulting from applying *K* = 4 (**left**) and *K* = 3 (**right**) when conducting the spatial partitional clustering.

References

1. Acevedo, S. *Gone with the Wind: Estimating Hurricane and Climate Change Costs in the Caribbean*; Working Paper No. 2016/199; International Monetary Fund: Washington, DC, USA, 2016.
2. Nurse, L.A.; McLean, R.F.; Agard Trinidad, J.; Pascal Briguglio, L.; Duvat-Magnan, V.; Pelesikoti, N.; Tompkins, E.; Webb, A. Small Islands. In *Climate Change 2014: Impacts, Adaptation, and Vulnerability. Part B: Regional Aspects. Contribution of Working Group II to the Fifth Assessment Report of the Intergovernmental Panel on Climate Change*; Barros, V.R., Field, C., Dokken, D.J., Mastrandrea, M.D., Dokken, D.J., Mach, K.J., Bilir, T.E., Chatterjee, M., Ebi, K.L., Estrada, Y.O., et al., Eds.; Cambridge University Press: Cambridge, UK; New York, NY, USA, 2014; pp. 1613–1654.

3. Wilkinson, E.; Arvis, B.; Mendler de Suarez, J.; Weingärtner, L.; Jaime, C.; Grainger, N.; Simonet, C.; Bazo, J.; Kruczkiewicz, A. *Preparing for Extreme Weather in the Eastern Caribbean*; Working Paper 603; Overseas Development Institute: London, UK, 2021.
4. Nugent, A.D.; Rios-Berrios, R. Factors Leading to Extreme Precipitation on Dominica from Tropical Storm Erika (2015). *Mon. Weather. Rev.* **2018**, *146*, 525–541. [CrossRef]
5. Pasch, R.J.; Penny, A.B.; Berg, R. *Hurricane Maria (AL152017)*; National Oceanic and Atmospheric Administration: Miami, FL, USA, 2017.
6. Pasch, R.J.; Penny, A.B. *Tropical Storm Erika (AL052015)*; National Oceanic and Atmospheric Administration: Miami, FL, USA, 2015.
7. NOAA. *How Do Hurricanes Form?* National Oceanic and Atmospheric Adminicstration: Miami, FL, USA, 2024.
8. Lin, Y.; Zhao, M.; Zhang, M. Tropical Cyclone Rainfall Area Controlled by Relative Sea Surface Temperature. *Nat. Commun.* **2015**, *6*, 6591. [CrossRef]
9. Lonfat, M.; Rogers, R.; Marchok, T.; Marks, F.D. A Parametric Model for Predicting Hurricane Rainfall. *Mon. Weather. Rev.* **2007**, *135*, 3086–3097. [CrossRef]
10. Ybañez, R. *Understanding Rainfall Return Periods Understanding Rainfall Return Periods*; University of the Philippines: Diliman, Quezon City, Philippines, 2013; Volume 1.
11. De Risi, R.; Jalayer, F.; De Paola, F.; Carozza, S.; Yonas, N.; Giugni, M.; Gasparini, P. From Flood Risk Mapping toward Reducing Vulnerability: The Case of Addis Ababa. *Nat. Hazards* **2020**, *100*, 387–415. [CrossRef]
12. Jetten, V.G. *CHaRIM Project Dominica National Flood Hazard Map Methodology and Validation Report*; University of Twente: Enschede, The Netherlands, 2016.
13. DMS. *Climatology for Canefield Airport 1982–2011*; Dominica Meteorological Service: Canefield, Dominica, 2012.
14. Smith, R.B.; Schafer, P.; Kirshbaum, D.J.; Regina, E. Orographic Precipitation in the Tropics: Experiments in Dominica. *J. Atmos. Sci.* **2009**, *66*, 1698–1716. [CrossRef]
15. Pollock, M.D.; O'Donnell, G.; Quinn, P.; Dutton, M.; Black, A.; Wilkinson, M.E.; Colli, M.; Stagnaro, M.; Lanza, L.G.; Lewis, E.; et al. Quantifying and Mitigating Wind-Induced Undercatch in Rainfall Measurements. *Water Resour. Res.* **2018**, *54*, 3863–3875. [CrossRef]
16. Veneziano, D.; Villani, P. Best Linear Unbiased Design Hyetograph. *Water Resour. Res.* **1999**, *35*, 2725–2738. [CrossRef]
17. Bezak, N.; Šraj, M.; Rusjan, S.; Mikoš, M. Impact of the Rainfall Duration and Temporal Rainfall Distribution Defined Using the Huff Curves on the Hydraulic Flood Modelling Results. *Geosciences* **2018**, *8*, 69. [CrossRef]
18. Balbastre-Soldevila, R.; García-Bartual, R.; Andrés-Doménech, I. A Comparison of Design Storms for Urban Drainage System Applications. *Water* **2019**, *11*, 757. [CrossRef]
19. Chow, V.T.; Maidment, D.R.; Mays, L.W. *Applied Hydrology*; McGraw-Hill: New York, NY, USA, 1998.
20. Lumbroso, D.M.; Boyce, S.; Bast, H.; Walmsley, N. The Challenges of Developing Rainfall Intensity-Duration-Frequency Curves and National Flood Hazard Maps for the Caribbean. *J. Flood Risk Manag.* **2011**, *4*, 42–52. [CrossRef]
21. Richard, C.Y.L.; Zhou, W.; Lee, T.C. Climatological Characteristics and Observed Trends of Tropical Cyclone–Induced Rainfall and Their Influences on Long-Term Rainfall Variations in Hong Kong. *Mon. Weather. Rev.* **2015**, *143*, 2192–2206.
22. Huffman, G.J.; Bolvin, D.T.; Braithwaite, D.; Hsu, K.L.; Joyce, R.J.; Kidd, C.; Nelkin, E.J.; Sorooshian, S.; Stocker, E.F.; Tan, J.; et al. Integrated Multi-Satellite Retrievals for the Global Precipitation Measurement (GPM) Mission (IMERG). *Adv. Glob. Chang. Res.* **2020**, *67*, 343–353.
23. Adhikari, A.; Liu, C.; Hayden, L. Uncertainties of GPM Microwave Imager Precipitation Estimates Related to Precipitation System Size and Intensity. *J. Hydrometeorol.* **2019**, *20*, 1907–1923. [CrossRef]
24. Wang, F. Temporal Pattern Analysis of Local Rainstorm Events in China During the Flood Season Based on Time Series Clustering. *Water* **2020**, *12*, 725. [CrossRef]
25. Cristiano, E.; ten Veldhuis, M.-C.; Gaitan, S.; Ochoa Rodriguez, S.; van de Giesen, N. Critical Scales to Explain Urban Hydrological Response: An Application in Cranbrook, London. *Hydrol. Earth Syst. Sci.* **2018**, *22*, 2425–2447. [CrossRef]
26. Santos, C.A.G.; Neto, R.M.B.; da Silva, R.M.; Costa, S.G.F. Cluster Analysis Applied to Spatiotemporal Variability of Monthly Precipitation over Paraíba State Using Tropical Rainfall Measuring Mission (TRMM) Data. *Remote Sens.* **2019**, *11*, 637. [CrossRef]
27. Ogden, F.L. Evidence of Equilibrium Peak Runoff Rates in Steep Tropical Terrain on the Island of Dominica during Tropical Storm Erika, August 27, 2015. *J. Hydrol.* **2016**, *542*, 35–46. [CrossRef]
28. DMS. *Rainfall Data on Tropical Storm, 26th to 27th August, 2015*; Dominica Meteorological Service: Canefield, Dominica, 2015.
29. GoCD. *Rapid Damage and Impact Assessment Tropical Storm Erika-August 27, 2015*; Government of the Commonwealth of Dominica: Roseau, Dominica, 2015.
30. EM-DAT. *Inventorying Hazards & Disasters Worldwide Since 1988*; EM-DAT: Brussels, Belgium, 2024.
31. Le, M.H.; Lakshmi, V.; Bolten, J.; Bui, D.D. Adequacy of Satellite-Derived Precipitation Estimate for Hydrological Modeling in Vietnam Basins. *J. Hydrol.* **2020**, *586*, 124820. [CrossRef]
32. Wang, Z.; Zhong, R.; Lai, C.; Chen, J. Evaluation of the GPM IMERG Satellite-Based Precipitation Products and the Hydrological Utility. *Atmos. Res.* **2017**, *196*, 151–163. [CrossRef]
33. Mekonnen, K.; Melesse, A.M.; Woldesenbet, T.A. Spatial Evaluation of Satellite-Retrieved Extreme Rainfall Rates in the Upper Awash River Basin, Ethiopia. *Atmos. Res.* **2021**, *249*, 105297. [CrossRef]

34. Cui, W.; Dong, X.; Xi, B.; Feng, Z.; Fan, J. Can the GPM IMERG Final Product Accurately Represent MCSs' Precipitation Characteristics over the Central and Eastern United States? *J. Hydrometeorol.* **2020**, *21*, 39–57. [CrossRef]
35. Tang, S.; Li, R.; He, J.; Wang, H.; Fan, X.; Yao, S. Comparative Evaluation of the GPM IMERG Early, Late, and Final Hourly Precipitation Products Using the CMPA Data over Sichuan Basin of China. *Water* **2020**, *12*, 554. [CrossRef]
36. Qi, W.; Yong, B.; Gourley, J.J. Monitoring the Super Typhoon Lekima by GPM-Based Near-Real-Time Satellite Precipitation Estimates. *J. Hydrol.* **2021**, *603*, 126968. [CrossRef]
37. NASA. *NASA Finds Heavy Rain in New Tropical Cyclone Hola near Vanuatu*; Goddard Space Flight Center: Greenbelt, MD, USA, 2018.
38. Omranian, E.; Sharif, H.O.; Tavakoly, A.A. How Well Can Global Precipitation Measurement (GPM) Capture Hurricanes? Case Study: Hurricane Harvey. *Remote Sens.* **2018**, *10*, 1150. [CrossRef]
39. NASA. *IMERG: Integrated Multi-satellitE Retrievals for GPM | NASA Global Precipitation Measurement Mission*; Goddard Space Flight Canter: Greenbelt, MD, USA, 2023.
40. Landsea, C.W.; Franklin, J.L. Atlantic Hurricane Database Uncertainty and Presentation of a New Database Format. *Mon. Weather. Rev.* **2013**, *141*, 3576–3592. [CrossRef]
41. Kisilevich, S.; Mansmann, F.; Nanni, M.; Rinzivillo, S. Spatio-Temporal Clustering. In *Data Mining and Knowledge Discovery Handbook*; Springer: Boston, MA, USA, 2009; pp. 855–874.
42. Wu, X.; Cheng, C.; Zurita-Milla, R.; Song, C. An Overview of Clustering Methods for Geo-Referenced Time Series: From One-Way Clustering to Co- and Tri-Clustering. *Int. J. Geogr. Inf. Sci.* **2020**, *34*, 1822–1848. [CrossRef]
43. Machiwal, D.; Dayal, D.; Kumar, S. Long-Term Rainfall Trends and Change Points in Hot and Cold Arid Regions of India. *Hydrol. Sci. J.* **2017**, *62*, 1050–1066. [CrossRef]
44. Hadi, A.F.; Yudistira, I.; Anggraeni, D.; Hasan, M. The Geographical Clustering of The Rainfall Stations on Seasonal GSTAR Modeling for Rainfall Forecasting. *J. Phys. Conf. Ser.* **2018**, *1028*, 012238. [CrossRef]
45. Alam, M.S.; Paul, S. A Comparative Analysis of Clustering Algorithms to Identify the Homogeneous Rainfall Gauge Stations of Bangladesh. *J. Appl. Stat.* **2019**, *47*, 1460–1481. [CrossRef]
46. Naranjo-Fernández, N.; Guardiola-Albert, C.; Aguilera, H.; Serrano-Hidalgo, C.; Montero-González, E. Clustering Groundwater Level Time Series of the Exploited Almonte-Marismas Aquifer in Southwest Spain. *Water* **2020**, *12*, 1063. [CrossRef]
47. Syakur, M.A.; Khotimah, B.K.; Rochman, E.M.S.; Satoto, B.D. Integration K-Means Clustering Method and Elbow Method for Identification of The Best Customer Profile Cluster. *IOP Conf. Ser. Mater. Sci. Eng.* **2018**, *336*, 012017. [CrossRef]
48. Kodinariya, T.M.; Makwana, P.R. Review on Determining of Cluster in K-Means Clustering. *Int. J. Adv. Res. Comput. Sci. Manag. Stud.* **2013**, *1*, 90–95.
49. Ketchen, D.J.; Shook, C.L. The Application of Cluster Analysis in Strategic Management Research: An Analysis and Critique. *Strateg. Manag. J.* **1996**, *17*, 441–458. [CrossRef]
50. Martin, J.E.; Sinclair, R.R. A Typology of the Part-Time Workforce: Differences on Job Attitudes and Turnover. *J. Occup. Organ. Psychol.* **2007**, *80*, 301–319. [CrossRef]
51. Feldmann, M.; Emanuel, K.; Zhu, L.; Lohmann, U. Estimation of Atlantic Tropical Cyclone Rainfall Frequency in the United States. *J. Appl. Meteorol. Climatol.* **2019**, *58*, 1853–1866. [CrossRef]
52. van Westen, C.J.; Alkema, D.; Damen, M.C.J.; Kerle, N.; Kingma, N.C. *Multi-Hazard Risk Assessment Distance Education Course Guide Book*; University of Twente: Enschede, The Netherlands, 2011.
53. van der Knijff, J.M.; Younis, J.; De Roo, A.P.J. LISFLOOD: A GIS-Based Distributed Model for River Basin Scale Water Balance and Flood Simulation LISFLOOD: A GIS-Based Distributed Model for River Basin Scale Water Balance and Flood Simulation. *Int. J. Geogr. Inf. Sci.* **2008**, *24*, 189–212. [CrossRef]
54. Mester, B.; Willner, S.N.; Frieler, K.; Schewe, J. Evaluation of River Flood Extent Simulated with Multiple Global Hydrological Models and Climate Forcings. *Environ. Res. Lett.* **2021**, *16*, 094010. [CrossRef]
55. Leijnse, T.; van Ormondt, M.; Nederhoff, K.; van Dongeren, A. Modeling Compound Flooding in Coastal Systems Using a Computationally Efficient Reduced-Physics Solver: Including Fluvial, Pluvial, Tidal, Wind- and Wave-Driven Processes. *Coast. Eng.* **2021**, *163*, 103796. [CrossRef]
56. van den Bout, B.; Jetten, V.G. The Validity of Flow Approximations When Simulating Catchment-Integrated Flash Floods. *J. Hydrol.* **2018**, *556*, 674–688. [CrossRef]
57. Delestre, O.; Cordier, S.; Darboux, F.; Du, M.; James, F.; Laguerre, C.; Lucas, C.; Planchon, O.; Cordier, S.; James, Á.F.; et al. FullSWOF: A Software for Overland Flow Simulation. In *Advances in Hydroinformatics*; Springer Hydrogeology: Singapore, 2013; pp. 221–231.
58. Umer, Y.M.; Jetten, V.G.; Ettema, J. Sensitivity of Flood Dynamics to Different Soil Information Sources in Urbanized Areas. *J. Hydrol.* **2019**, *577*, 123945. [CrossRef]
59. Umer, Y.M.; Jetten, V.G.; Ettema, J.; Lombardo, L. Application of the WRF Model Rainfall Product for the Localized Flood Hazard Modeling in a Data-Scarce Environment. *Nat. Hazards* **2022**, *111*, 1813–1844. [CrossRef]
60. van den Bout, B.; Jetten, V.G. Catchment-Scale Multi-Process Modeling with Local Time Stepping. *Environ. Earth Sci.* **2020**, *79*, 184. [CrossRef]
61. Baartman, J.E.M.; Jetten, V.G.; Ritsema, C.J.; de Vente, J. Exploring Effects of Rainfall Intensity and Duration on Soil Erosion at the Catchment Scale Using OpenLISEM: Prado Catchment, SE Spain. *Hydrol. Process* **2012**, *26*, 1034–1049. [CrossRef]

62. Starkloff, T.; Stolte, J.; Hessel, R.; Ritsema, C.; Jetten, V.G. Integrated, Spatial Distributed Modelling of Surface Runoff and Soil Erosion during Winter and Spring. *Catena* **2018**, *166*, 147–157. [CrossRef]
63. van den Bout, B.; van Westen, C.J.; Jetten, V.G. Non-Monotonic Relationships between Return Periods of Precipitation Surface Hazard Intensity. *Water* **2022**, *14*, 1348. [CrossRef]
64. Serere, H.N. *Developing a Worst-Case Tropical Cyclone Rainfall Scenario for Flood on Dominica*; Faculty of Geo-Information Science and Earth Observation of the University of Twente: Enschede, The Netherlands, 2020.
65. Paul-Rolle, A. *Commonwealth of Dominica Disaster Risk Reduction Country Profile*; Office for Disaster Management: Roseau, Dominica, 2014.
66. Barclay, J.; Wilkinson, E.; White, C.S.; Shelton, C.; Forster, J.; Few, R.; Lorenzoni, I.; Woolhouse, G.; Jowitt, C.; Stone, H.; et al. Historical Trajectories of Disaster Risk in Dominica. *Int. J. Disaster Risk Sci.* **2019**, *10*, 149–165. [CrossRef]
67. Matyas, C.J. Quantifying the Shapes of U.S. Landfalling Tropical Cyclone Rain Shields. *Prof. Geogr.* **2007**, *59*, 158–172. [CrossRef]
68. Ayala, J.J.; Matyas, C.J. Tropical Cyclone Rainfall over Puerto Rico and Its Relations to Environmental and Storm-specific Factors. *Int. J. Climatol.* **2016**, *36*, 2223–2237. [CrossRef]
69. van Westen, C.J. *National Scale Landslide Susceptibility Assessment for Dominica*; University of Twente: Enschede, The Netherlands, 2016.
70. Rouse, W.C.; Reading, A.J.; Walsh, R.P.D. Volcanic Soil Properties in Dominica, West Indies. *Eng. Geol.* **1986**, *23*, 1–28. [CrossRef]
71. Llasat, M. An Objective Classification of Rainfall Events on the Basis of Their Convective Features: Application to Rainfall Intensity in the Northeast of Spain. *Int. J. Climatol.* **2001**, *21*, 1385–1400. [CrossRef]
72. Dilmi, M.D.; Mallet, C.; Barthes, L.; Chazottes, A. Data-Driven Clustering of Rain Events: Microphysics Information Derived from Macro-Scale Observations. *Atmos. Meas. Tech.* **2017**, *10*, 1557–1574. [CrossRef]
73. Zhang, Y.; Moges, S.; Block, P. Optimal Cluster Analysis for Objective Regionalization of Seasonal Precipitation in Regions of High Spatial–Temporal Variability: Application to Western Ethiopia. *J. Clim.* **2016**, *29*, 3697–3717. [CrossRef]
74. Chen, L.; Chen, Y.; Zhang, Y.; Xu, S. Spatial Patterns of Typhoon Rainfall and Associated Flood Characteristics over a Mountainous Watershed of a Tropical Island. *J. Hydrol.* **2022**, *613*, 128421. [CrossRef]
75. Zhou, Y.; Matyas, C.J. Spatial Characteristics of Rain Fields Associated with Tropical Cyclones Landfalling over the Western Gulf of Mexico and Caribbean Sea. *J. Appl. Meteorol. Climatol.* **2018**, *57*, 1711–1727. [CrossRef]
76. Zagrodnik, J.P.; Jiang, H. Investigation of PR and TMI Version 6 and Version 7 Rainfall Algorithms in Landfalling Tropical Cyclones Relative to the NEXRAD Stage-IV Multisensor Precipitation Estimate Dataset. *J. Appl. Meteorol. Climatol.* **2013**, *52*, 2809–2827. [CrossRef]
77. Matyas, C.J. Conditions Associated with Large Rain-Field Areas for Tropical Cyclones Landfalling over Florida. *Phys. Geogr.* **2014**, *35*, 93–106. [CrossRef]